Gain by Mixture-based Image Segmentation for Virtual Colonoscopy with Colonic Material Tagging

Lihong Li[1,2], Su Wang[1], Zigang Wang[1], Jing Wang[1], Hongbing Lu[3], and Zhengrong Liang[1]

[1] Department of Radiology, State University of New York, Stony Brook, NY 11794, USA
[2] Department of Engineering Science and Physics, College of Staten Island of the City University of New York, Staten Island, NY 10314, USA
[3] Department of Biomedical Engineering/Computer Application, Fourth Military Medical University, Xi'an, Shaanxi 710032, China

ABSTRACT

Computed tomography-based virtual colonoscopy or CT colonography (CTC) currently utilizes oral contrast solution to differentiate the colonic fluid and possibly residual stool from the colon wall. The enhanced image density of the tagged colonic materials causes a significant partial volume (PV) effect into the colon wall as well as the lumen space (air or CO_2). The PV effect into the colon wall can "bury" polyps of small size by increasing their image densities to a noticeable level, resulting in false negatives. It can also create false positives when PV effect goes into the lumen space. Modeling the PV effect for mixture-based image segmentation has been a research topic for many years. This paper presents the practical implementation of our newly developed statistical image segmentation framework, which utilizes the EM (expectation-maximization) algorithm to estimate (1) tissue fractions in each image voxel and (2) statistical model parameters of the image under the principle of maximum *a posteriori* probability (MAP). This partial-volume expectation-maximization (PV-EM) mixture-based MAP image segmentation pipeline was tested on 52 CTC datasets downloaded from the website of the VC Screening Resource Center, with each dataset consisting of two scans of supine and prone positions, resulting in 104 CT volume images. The cleansed lumens by the automated PV-EM image segmentation algorithm were visualized with comparison to our previous work, with the gain achieved mainly in the following three aspects: (1) the tissue fraction information of those voxels with PV effect have been well preserved, (2) the problem of incomplete cleansing of tagged materials in our previous work has been mitigated, and (3) the interference caused by small bowel was significantly released.

Keywords: PV effect, tissue mixture, EM algorithm, parameter estimation, MAP image segmentation, electronic colon cleansing.

1. INTRODUCTION

Virtual colonoscopy (VC) [1,2] is known to be an emerging method utilizing advanced medical imaging and computer technologies to mimic the fiber optic colonoscopy (OC) navigation procedue, looking for polyps via fly-through in a virtual colon model which is constructed from patient abdominal images. Compared to OC, VC has demonstrated the potential to become a mass screening modality in terms of safety, cost and patient compliance [3]. By the use of oral contrast to tag the colonic materials, the residue stool and fluid have an enhanced image density compared to the surrounding colon/polyp tissues such that electronic colon cleansing (ECC) becomes a new technology [4] and has been integrated into a commercial VC system to identify the enhanced colonic materials and restore a "cleansed" colon model for both VC navigation [3,5,6] and following-up computer-aided detection (CAD) analysis [7]. It has been demonstrated that ECC is able to provide a comparable performance as the routine OC in detecting clinically significant polyps of size greater than 8mm [8,9].

Image segmentation plays an important role in the ECC new technology. However, the traditional image segmentation of labeling each image voxel as a single tissue type ignores the partial volume (PV) effect and, therefore, losses the

[1] Email: jzl@mil.sunysb.edu; Phone: (631) 444-7837; Fax: (631) 444-6450.

Medical Imaging 2007: Physiology, Function, and Structure from Medical Images, edited by Armando Manduca, Xiaoping P. Hu, Proc. of SPIE Vol. 6511, 65110V, (2007) · 1605-7422/07/$18 · doi: 10.1117/12.708927

details on the colon mucosa where most voxels contain more than one tissue types. Ignoring the PV effect could be an essential factor of missing detection of small polyps. Progress has been made by soft image segmentation, which seeks the probability of a tissue type in a voxel while retaining the tissue labels of the traditional hard segmentation [2,6]. Directly modeling the tissue mixtures in each image voxel for an explicit solution of the PV effect has been a research interest for many years [10-13]. This paper presents the practical implementation details of an newly developed PV image segmentation pipeline [13,14], utilizing the expectation-maximization (EM) algorithm [15] to estimate simultaneously (1) tissue fractions in each image voxel and (2) statistical model parameters of the image data under the principle of maximuma posteriori probability (MAP). In doing so, the PV effect is modeled in a continuous space and estimated directlyas the fraction of each tissue type in the original voxel. Fifty-two CTC datasets downloaded from the website of the VC Screening Resource Center are utilized to evaluate the PV-EM image segmentation pipeline in a way that the obtained cleansed lumens are visualized with comparison to our previous work [5,6]. The gain achieved by the PV-EM image segmentation pipeline is mainly in the following three aspects: (1) the tissue fraction information of those voxels with PV effect have been well preserved, (2) the problem of incomplete cleansing of tagged material in our previous work [5,6] has been mitigated, and (3) the interference caused by small bowel and remaining bone is significantly released.

The reminder of this paper is ogranized as follows. Section II briefly introduces the PV-EM algorithm, and followed by Section III where more practical implementation detailes of our newly developed PV-EM image segmentation pipeline are fully described. Section IV then validates our method using 52 VC datasets, highlighting the major contributions of our new method compared to our previous work. Finally, Section V draws some conclusions.

2. PARTIAL VOLUME-EXPECTATION MAXIMIZATION ALGORITHM

In this section, the PV-EM algorithm is briefly introduced based on the assumption that the acquired CT image **Y** reflects the distribution of *K* tissue types inside the body. In other words, there are *K* possible tissue types within each image voxel, where each tissue type has a contribution to the observed image density value Y_i at voxel *i*.

2.1 Image Data Model

It is assumed that the acquired image **Y** is represented by a column vector into the form of $\{Y_i, i = 1, \ldots, I\}$ where *I* denotes the total number of voxels in the image and each Y_i is an observation of a random variable with mean $\overline{Y}_i$ and variance σ_i^2, i.e.,

$$Y_i = \overline{Y}_i + n_i . \tag{1}$$

If we further assume that noise $n_i, i = 1, \ldots, I$, is statistically mutually independent and follows a Gaussian distribution with zero mean and variance σ_i^2, then given all the mean and variance distribution $\{\overline{Y}_i, i = 1, \ldots, I\}$ and $\{\sigma_i^2, i = 1, \ldots, I\}$ respectively, the conditional probability distribution of the acquired image **Y** is described as follows

$$p(\mathbf{Y} \mid \{\overline{Y}_i\}, \{\sigma_i^2\}) = \prod_{i=1}^{I} p(Y_i \mid \overline{Y}_i, \sigma_i^2) . \tag{2}$$

It should be noted that each voxel in many medical imaging applications can have more than one tissue types due to the limited spatial resolution such that ignorance of the substructures within each voxel will suffer from the well-known PV effect. In what follows, a more detailed mixture model within each voxel would be briefly introduced as opposed to the global structures using model parameters $\{\overline{Y}_i\}$ and $\{\sigma_i^2\}$ with $i = 1, \ldots, I$ as described by (1).

2.2 Tissue Mixture Model

There are probably *K* tissue types within each voxel $\{Y_i, i = 1, \ldots, I\}$, where the contribution of tissue type k to the observation of Y_i is denoted by $\{X_{ik}, i=1,\ldots,I; k=1,\ldots,K\}$. It is obvious that X_{ik} is also a random variable around mean $\overline{X}_{ik}$ and variance σ_{ik}^2, i.e.,

$$X_{ik} = \overline{X}_{ik} + n_{ik} \tag{3}$$

where the noise $\{n_{ik}, i=1,\ldots,I; k=1,\ldots,K\}$ is statistically independent to each other and follows a Gaussian distribution with zero mean and variance σ_{ik}^2. Following the same argument on the image data model, given the tissue mixture model parameters $\{\overline{X}_{ik}, i=1,\ldots,I; k=1,\ldots,K\}$ and $\{\sigma_{ik}^2, i=1,\ldots,I; k=1,\ldots,K\}$, we have

$$p(\mathbf{X} \mid \{\overline{X}_{ik}\}, \{\sigma_{ik}^2\}) = \prod_{i=1}^{I} \prod_{k=1}^{K} p(X_{ik} \mid \overline{X}_{ik}, \sigma_{ik}^2). \tag{4}$$

As a result, the tissue mixture model within each voxel $\{Y_i, i=1,\ldots,I\}$ by accounting for the contribution of each tissue type $\{X_{ik}, i=1,\ldots,I; k=1,\ldots,K\}$ is depicted as follows

$$Y_i = \sum_{k=1}^{K} X_{ik}, \quad n_i = \sum_{k=1}^{K} n_{ik} \quad \text{and} \quad \sigma_i^2 = \sum_{k=1}^{K} \sigma_{ik}^2. \tag{5}$$

More specifically, if Z_{ik} is assumed to be the contribution fraction of tissue type k in voxel Y_i with $\sum_{k=1}^{K} Z_{ik} = 1,\ 0 \le Z_{ik} \le 1$, also μ_k and ν_k be the mean and variance of tissue type k fully filling in voxel Y_i, then we have the following relationship as well

$$\begin{aligned} \overline{X}_i &\overset{def}{=} Z_{ik}\mu_k, \quad \sigma_{ik}^2 \overset{def}{=} Z_{ik}\nu_k \\ \overline{Y}_i &= \sum_{k=1}^{K} Z_{ik}\mu_k, \quad \sigma_i^2 = \sum_{k=1}^{K} Z_{ik}\nu_k \end{aligned} \tag{6}$$

In doing so, (2) can be rewritten as

$$p(\mathrm{Y} \mid \{\mu_k\}, \{\nu_k\}, \{Z_{ik}\}) = \prod_{i=1}^{I} \frac{1}{\sqrt{2\pi \sum_{k=1}^{K} Z_{ik}\nu_k}} \exp\left\{ - \frac{(Y_i - \sum_{k=1}^{K} Z_{ik}\mu_k)^2}{2\sum_{k=1}^{K} Z_{ik}\nu_k} \right\}. \tag{7}$$

The maximum likelihood (ML) solution on the Gaussian distribution $\{Y_i, i=1,\ldots,I\}$ of (7) for fractions $\{Z_{ik}, i=1,\ldots,I; k=1,\ldots,K\}$ can be computed, given the model parameters μ_k and ν_k with $k=1,\ldots,K$. However, solving the optimization problem can be very complicated due to the fact that simultaneous estimation of both $\{Z_{ik}, i=1,\ldots,I; k=1,\ldots,K\}$ and μ_k and ν_k with $k=1,\ldots,K$ is numerically intractable. As a result, the EM algorithm is considered as an alternative but effective solution, with the mixture model as described by (5) being re-interpreted as a many-to-one mapping problem of missing data.

2.3 Priori Model for Mixture Regularization

So far, all we discussed is based on maximum-likelihood expectation-maximization (ML-EM) framework, which is known to yield noisy segmentation as the iteration number increases [16]. As far as image segmentation is concerned, many literatures have evicted the strength of maximum *a posteriori*-expectation maximization (MAP-EM) or penalized ML (pML) algorithm by introducing a Markov random field (MRF) penalty term to define an *a priori* distribution for the tissue mixture fraction around its neighboring voxels, such that ML-EM becomes MAP-EM by the use of the Bayesian theory. Based upon the priori knowledge of what each voxel's neighboring voxels are mostly look like, the MAP-EM is capable to provide much more smooth parameter estimation for the tissue type mixture fraction Z_{ik} to achieve image segmentation, recovering those fraction information Z_{ik} on the boundary or region with significant PV effect.

By a Gibbs model on the Markov random field (MRF) framework, the penalty on the tissue mixture parameter Z_{ik} has the following general form

$$P\left(Z_{ik} \mid \{Z_{ik\varepsilon_i}\}\right) = C^{-1} \times \exp[-\beta U(Z_{ik} - Z_{ik\varepsilon_i})] \tag{8}$$

where $\{Z_{ik\varepsilon_i}\}$ are the surrounding neighbor voxels of Z_{ik} in the neighboring system ε_i, C is a normalization constant and β is an adjustable parameter controlling the degree of the penalty. The exponential function $U(.)$ can be written as a quadratic form like

$$U(Z_{ik}) = \sum_{r \in \varepsilon_i} w_{ir} \cdot (Z_{ik} - Z_{rk})^2 \tag{9}$$

where w_{ir} is a weighing factor for different orders of neighbors. As a result, our PV-EM algorithm for the MAP solution consists of the following two steps of the EM algorithm[15] below.

(1) E-step: the conditional expectation at the *n*-th iteration is calculated by

$$\begin{aligned} Q(\Theta \mid \Theta^{(n)}) &= \mathrm{E}[\ln\, p(\mathrm{X} \mid \Theta) \cdot p(Z) \mid Y, \Theta^{(n)}] \\ &= -\frac{1}{2} \sum_{i,k} \{\ln(2\pi) + \ln(Z_{ik}\nu_k) + \frac{1}{Z_{ik}\nu_k}[(X_{ik}^2)^{(n)} - 2X_{ik}^{(n)} Z_{ik}\mu_k + Z_{ik}^2\mu_k^2] + U(Z_{ik})\} \end{aligned} \tag{10}$$

where parameter set Θ represents the fractions $\{Z_{ik}\}$ and tissue parameters $\{\mu_k, \nu_k\}$, and $X_{ik}^{(n)}$ and $(X_{ik}^2)^{(n)}$ are the conditional expectations of X_{ik} and X_{ik}^2 respectively

$$X_{ik}^{(n)} = \mathrm{E}[X_{ik} \mid Y_i, \Theta^{(n)}] = Z_{ik}^{(n)}\mu_k^{(n)} + \frac{(Z_{ik}\nu_k)^{(n)}}{\sum_{j=1}^{K}(Z_{ij}\nu_j)^{(n)}} \cdot (Y_i - \sum_{j=1}^{K} Z_{ij}^{(n)}\mu_j^{(n)}) \tag{11}$$

$$(X_{ik}^2)^{(n)} = \mathrm{E}[X_{ik}^2 \mid Y_i, \Theta^{(n)}] = (X_{ik}^{(n)})^2 + (Z_{ik}\nu_k)^{(n)} \cdot \frac{\sum_{j\neq k}^{K}(Z_{ij}\nu_j)^{(n)}}{\sum_{j=1}^{K}(Z_{ij}\nu_j)^{(n)}}. \tag{12}$$

where $(X_{ik}^2)^{(n)}$ is the square of the *n*-th iterated estimate of $X_{ik}^{(n)}$.

(2) M-step: the maximization of the conditional expectation determines the (*n*+1)-th iterated results for the fractions and model parameters. For the mean parameter μ_k, we have

$$\mu_k^{(n+1)} = \frac{\sum_i X_{ik}^{(n)}}{\sum_i Z_{ik}}. \tag{13}$$

Similarly for the variance parameter ν_k, we have

$$\nu_k^{(n+1)} = \frac{1}{I}\sum_i \frac{(X_{ik}^2)^{(n)} - 2X_{ik}^{(n)} Z_{ik}^{(n)}\mu_k^{(n)} + (Z_{ik}^2\mu_k^2)^{(n)}}{Z_{ik}^{(n)}}. \tag{14}$$

For mixture of two tissue types in each voxel, the fractions $\{Z_{ik}\}$ can be estimated by [14]

$$Z_{i1}^{(n+1)} = \frac{X_{i1}^{(n)}(\sigma_{i2}^2)^{(n)}\mu_1^{(n)} + (\mu_2^2)^{(n)}(\sigma_{i1}^2)^{(n)} - X_{i2}^{(n)}(\sigma_{i1}^2)^{(n)}\mu_2^{(n)} + 4\beta(\sigma_{i1}^2)^{(n)}(\sigma_{i2}^2)^{(n)}\sum w_{ir} Z_{r1}^{(n)}}{(\mu_1^2)^{(n)}(\sigma_{i2}^2)^{(n)} + (\mu_2^2)^{(n)}(\sigma_{i1}^2)^{(n)} + 4\beta(\sigma_{i1}^2)^{(n)}(\sigma_{i2}^2)^{(n)}\sum w_{ir}} \tag{15}$$

where $Z_{i2}^{(n+1)} = 1 - Z_{i1}^{(n+1)}$ and $\sigma_{ik}^2 = Z_{ik}\nu_k$.

3. IMPLEMENTATION DETAILS OF THE PV-EM ALGORITHM

It has been demonstrated that our previous PV-EM pipeline is successful in segmenting the entire colon lumen from original CT image, cleansing the colon lumen and restoring the CT density values of the colon tissue in the enhanced mucosa layer [9,14]. However, there are still some implementation details worthy to be mentioned as follows.

3.1 The full use of tissue fraction information Z_{ik} to maximally reduce the computational complexity while maintaining the consistency between two consecutive EM iterations

A new strategy to update the tissue fraction Z_{ik} associate with tissue type *k* within voxel *i* is developed according to the following criterion:

$$Z_{ik} = 0, \quad if \left(\frac{Z_{ik} + \sum_{j \in N(i)} w_j Z_{jk}}{Z_{ik} + \sum_{k=1}^{K} \sum_{j \in N(i)} w_j Z_{jk}} \right) \leq \varepsilon \tag{16}$$

where $N(i)$ denotes the second-order neighborhood system centered at voxel *i* and w_j is a scale factor reflecting the difference among different orders of the neighboring voxels. By means of (16), the contributions made by different tissue types are sorted in a descending order, such that least-important tissue type can be ignored from the next PV-EM iteration. As a result, re-labeling each voxel is able to indicate the actual number of tissues present in voxel *i*.

The major advantage provided by (16) is due to the fact that the soft fraction information of Z_{ik} in voxel *i* is significantly preserved during each iterative step in the sense that Z_{ik} is smoothly changed depending upon its surrounding neighbors as the number of iterations increases, efficiently avoiding the sudden change of Z_{ik} from *n*-th to (*n*+1)-th iteration in our previous work. On the other hand, the computational complexity due to the occurrence of more than two tissue types within one voxel can be released.

3.2 The use of vector quantification to compensate for the ignorance of soft-tissue structures during the hard segmentation initialization step

It has been demonstrated that the PV-EM algorithm is local maximum and hence the final convergence appears to be more sensitive to the initialization model parameter[14]. Two kinds of parameters are needed to be initialized to start the PV-EM algorithm: the model parameters specified by $\{\mu_k, \nu_k\}$ for each tissue type and the tissue mixture fraction denoted by Z_{ik}. Experimental results [14] have also demonstrated that the iterative processes of the PV-EM algorithm is not sensitive to the initial model parameters in the sense that even when the initial means and variances $\{\mu_k^{(0)}, \nu_k^{(0)}\}$ were added by 10% more errors, the PV-EM algorithm still converged to the good results. To the contrary, the PV-EM algorithm convergence appears to be more sensitive to the initial estimate of the tissue mixture fraction $Z_{ik}^{(0)}$. In what follows, this paper presents a vector quantification (VQ)-based initialization method, aiming to preserve the PV effect by taking into account the neighboring voxels.

As an image compression algorithm, VQ has received considerable interest and been used in many applications such as image and voice compression and classification, statistic pattern recognition. As its name implied, the use of VQ in CT images is limited since each voxel in CT images has only one value uniquely representing it. Several modifications have been made to the explanation and reformation of CT images to fit into the framework of VQ. For example, Chen *et al.* [5] has proposed a novel method of grouping the intensities of those 23 voxels in a local volume to form a twenty-three dimensional (23-D) local intensity vector to achieve the classification of the body voxels based on the intensity similarity within certain spatial range [5]. As a result, each voxel is reinterpreted as a 23-D local intensity vector, such that the computational complexity is expected to be very high since each CT image consists of millions of body voxels. To reduce the computing burden, principal component analysis (PCA) has been also applied to the local vector series to determine the dimension of the feature vectors. Moreover, the results of PCA on the datasets of the training samples showed that a reasonable dimension of the feature vectors was 5, where the summation of the first five principle components' variances was more than 92% of the total variance [5]. Different from Chen *et al.*'s work where VQ is implemented in a two-stage manner to segment the entire colon lumen, the idea of VQ is incorporated into our PV-EM pipeline under the assistance of thresholding hard segmentation. It is expected to provide much more detailed information about the difference between submerged soft-tissue structure, tagged material, degraded tagged material, as well as the bone. The VQ-based initialization method is briefly summarized into the following steps.

(1) The whole boy image is firstly divided into four different classes, air (including lung), muscle, tissue and bone (including tagged material, submerged soft-tissue structure) through hard segmentation by the use of pre-defined thresholds.

(2) For bone class only, each voxel belonging to this class is re-interpreted as a 23-D local intensity vector, followed by PCA transform through eigen-value decomposition, only using the first five principle components to uniquely

represent the original 23-D local intensity vector. In other words, those voxels belonging to bone class have been translated into a 5-D local intensity vector with each dimension coming from a distinct principle component.

(3) The VQ is then applied to these reformed bone class voxels, finding representative 5-D vectors for each sub-divided bone classes. A practical issue then arises, which is how to determine the number of sub-divided bone classes. In our study, we follow the same track by further dividing the bone class into 10 sub-classes through an unsupervised self-adaptive VQ algorithm [5]. Further experiments have demonstrated that the number of 10 is sufficient to fully describe the characteristics of the bone, tagged material, submerged soft-tissue structure and even the degraded tagged material whose intensity is much lower than the normal tagged material.

If we initially label air class as 1, muscle class as 2, tissue class as 3, and the original bone class as 4, then the new label results obtained from VQ 10-class sub classification can be summarized by Table 1 as follows.

Table 1: label results derived from initial hard segmentation and followed by 10-class VQ classification

	Before VQ	After VQ	
AIR	1	1	
MUSCLE	2	2	
TISSUE	3	3	
BONE	4	Sub-class 1	5
		Sub-class 2	6
		Sub-class 3	7
		Sub-class 4	8
		Sub-class 5	9
		Sub-class 6	10
		Sub-class 7	11
		Sub-class 8	12
		Sub-class 9	13
		Sub-class 10	14

More comments are worthwhile to be mentioned. Each voxels initially belonging to bone class is re-grouped into 10 sub-classes by the VQ classification. In doing so, the means of 10 sub-classes, denoted by $m_k, k = 1,\ldots 10$, can be accordingly calculated and also sorted in an increasing order. As a result, the new labels from 5-14 are capable of indicating what kind of material a bone-class voxel is mostly like to be. In other words, if a bone-class voxel is relabeled as 5 after VQ, then it is more likely to be a submerged soft-tissue structure. However, if it is relabeled as 14 instead, we would say it has high probability to be claimed as pure bone or pure tagged material. As for the label between 5 and 14, it serves as an indicator to provide more details on which direction it tends to behave, i.e., the larger the label, the more likely to be like pure bone/tagged material, and the smaller the label, the more likely to behave like soft-tissue structure or even degraded tagged materials.

Under the assistance of such detailed information within bone class, the initialization strategy can be modified in a way that the model parameters $\{\mu_k^{(0)}, \nu_k^{(0)}\}$ are still determined by hard segmentation since they have little effect on the convergence of the PV-EM algorithm, while for the tissue mixture fracture $Z_{ik}^{(0)}$, the newly VQ-generated labels from 5-14 are serving as indicators, re-assigning different weights reflecting different contribution made by the soft-tissue structure or the pure bone. More specifically, the larger the label of tissue type *k* within voxel *i*, the more $Z_{ik}^{(0)}$ and vice versa.

3.3 The post-processing steps to remove the interference caused by small bowel, lung and bone

Since colon is not the only gas-filled structure in the abdomen, there exists inevitable interference caused by small bowel, accordingly increasing the false positives especially when the folders inside the small bowel mimic. As a complementary post-processing step to our PV-EM image segmentation pipeline, removing small bowel as well as other interfering structures such as the bone and lungs, becomes vital to the follow-up CAD to locate polyps. A connected component-based small bowel removal method is summarized into the following steps.

(1) Morphological erosion operation is firstly employed to shrink the whole colon area, such that only those voxels without PV effect, i.e., mixing fractions Z_{ik} for colon structure is 100%, are preserved for the next step.

(2) Connected component analysis is applied to each pure colon voxel. In doing so, the pure colon area is divided into several separate connected components with different sizes through 3-D region growing.

(3) If we further assume that colon is connected as a whole and considered as the largest connected component in the abdomen, then the easiest way to remove other interference such as the small bowel is to select the largest connected component, while ignoring the remaining separate components. However, this assumption is not valid through all the cases. We found that almost in 30% abnormal cases, colon is blocked into several separate components as well. In order to mitigate this problem, choosing the several largest components turns out to be an alternative method. Through our comprehensive experiments, the number of components to be selected is no more than 3 in 99% cases.

(4) After choosing the largest connected component for the normal case or 3 components for the abnormal cases, colon and small bowel can be successfully divided apart. Recovering those voxels with PV effect through morphological dilation becomes the final step as a pair-wise operation to the erosion in the very first step. The layers for dilation were empirically set to be 3-5 which covers the thickness of the mucosa layer.

The connected component-based small bowel removal method outlined by steps (1)-(4) above works efficiently in removing interfering structures such as the small bowel, remaining bone and even stripe noise in the sense that almost 90% small bowel can be removed without any loss of colon information. Most importantly, the PV effect, which is derived from our proposed PV-EM image segmentation iterative algorithm are well preserved as a benefit to the follow-up CAD detection.

4. EXPERIMENTAL RESULTS

This paper tabulates the preliminary evaluation of the improved PV-EM image segmentation pipeline above for mixture image segmentation and electronic colon cleansing by 52 CTC datasets, downloaded from the website of the VC Screening Resource Center consists. Each of the 52 VC datasets consists of two CT scans, supine and prone views, both of which represented by a volume image of more than 300 slices of 512×512 array size.

4.1 Convergence speed of the PV-EM algorithm

In what follows, equation (17) defines the criterion of stopping rule for the PV-EM image segmentation algorithm as

$$Max\left(\left|\frac{\mu_k^{(n+1)}}{\mu_k^{(n)}}-1\right|_{k=1,2,3,4}\right)\le\delta \tag{17}$$

where the maximum ratios of class mean difference between the (n+1)-th and the n-th iterations to the n-th class mean itself among all the four different tissue types is less than the threshold δ as specified by the user. In this study, the threshold δ was set to be 0.05. Taking the dataset (named as the number 043 at the website of the VC Screening Resource Center) at prone position as an example to illustrate the converging speed of the PV-EM algorithm, Fig. 1 shows the changing rate of mean values versus the iteration numbers.

As shown in Fig.1, the PV-EM image segmentation algorithm usually takes 9 or 10 iterations to reach the optimum points as stopping rule defined by (17) if the threshold δ is set to be 0.05. However in practice, we usually set the number of iterations to be 4, which is sufficient in terms of preserving PV effect. In other words, after 4 iterations, the curve describing the converging speed of the PV-EM algorithm has already reflected an obvious descending tendency. In doing so, computational time can be dramatically reduced without any significant loss of PV information.

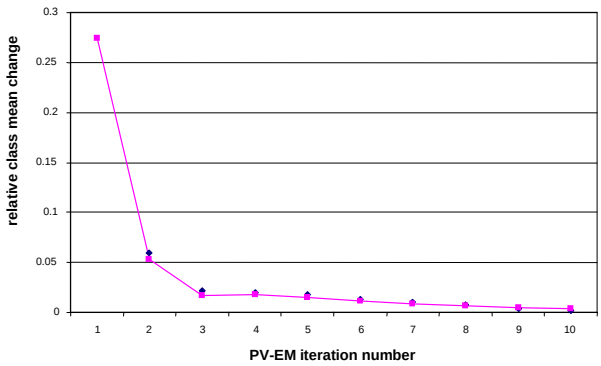

Figure 1: The converging speed of PV-EM algorithm

4.2 Capability of preserving the PV effect

Compared to our previous soft-segmentation work[6], the PV effect has been well preserved by our newly developed PV-EM image segmentation algorithm. Instead of nearly hard segmentation, the PV-EM algorithm is capability to provide soft tissue mixture information to fully describe the PV effect. As shown in Fig. 2, the mixing fraction Z_{ik} for colon structure is smoothly changing from 100% (corresponding to pure colon area) down to 0% covering a typical mucosa layer within 3-5 pixel thickness.

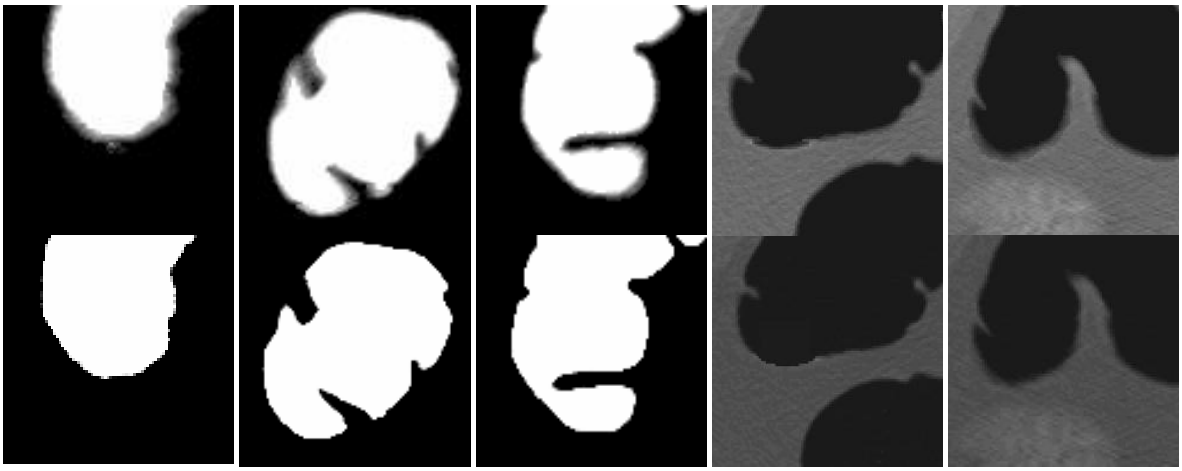

Figure 2: Comparison between our improved PV-EM pipeline and our previous soft-segmentation work in dealing with the PV-EM effect. The pictures at the top row are the segmentation as well as the cleansed results from our improved pipeline and those results obtained by our previous work are shown in the bottom row.

4.3 Capability of complete electronic cleansing

Another advantage of our PV-EM image segmentation algorithm over our previous work [6] is in the capability of complete electronic cleansing. Compared to our previous work [6] where there is some tagged material remaining in the cleansing results, burying some of the folders and increasing the false negative probability, our PV-EM image segmentation algorithm overcomes this problem by completely cleansing the tagged materials while leaving small colon folders untouched, see Fig.3.

4.4 Capability of removing interferences caused by the small bowel and the remaining bone

Figure 4 is also included here to illustrate the difference between our PV-EM image segmentation algorithm and our previous soft-segmentation work [6] in terms of the capability of removing interferences caused by the small bowel as well as the remaining bone. As we mentioned earlier, successful removal of the small bowel and the remaining bone is able

to save much of the computational time required by the follow-up CAD polyp detection, while effectively reducing the false positive probability.

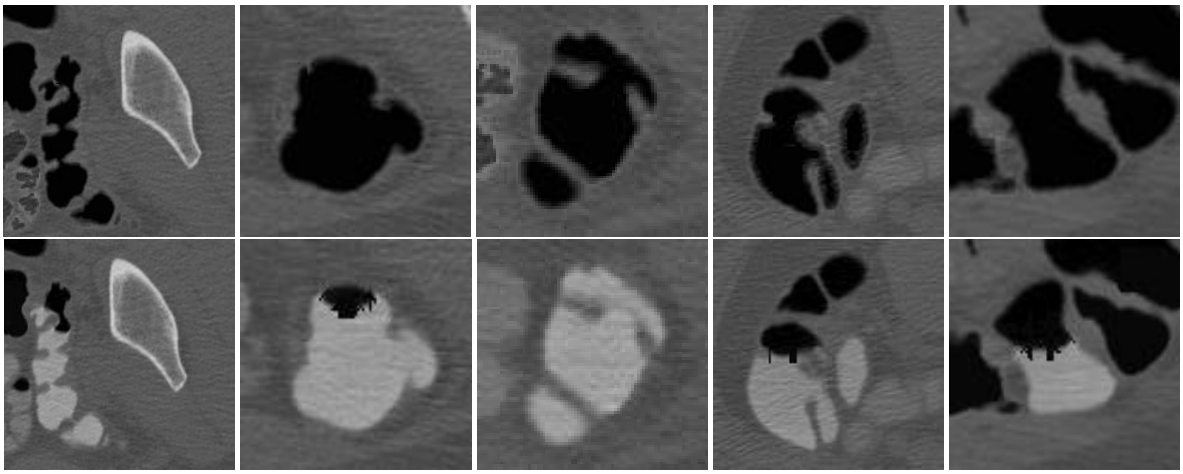

Figure 3: Comparison between our improved PV-EM pipeline and our previous soft-segmentation work in electronic colon cleansing. The pictures at the top row are segmentation results from our improved pipeline and the results obtained by our previous work are shown in the bottom row.

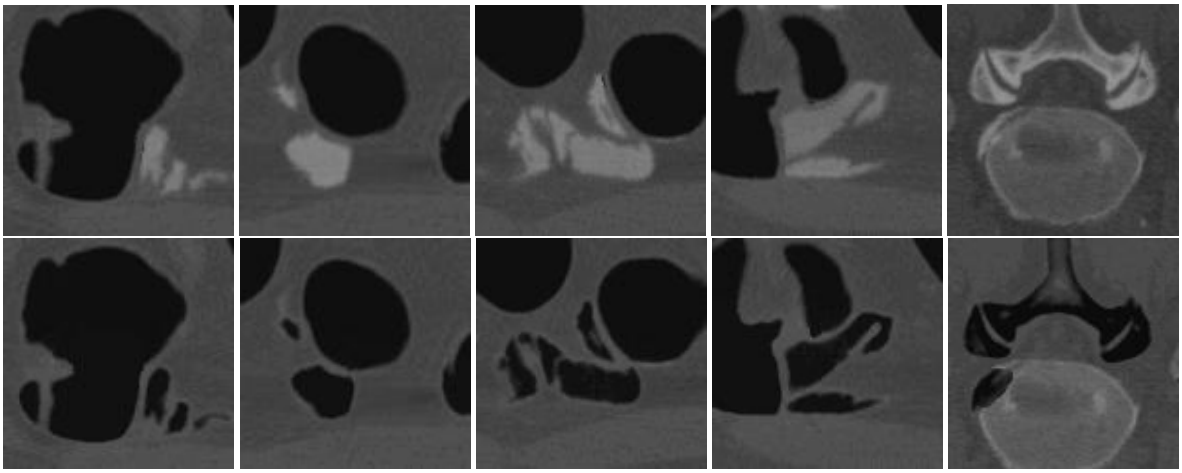

Figure 4. Comparison between our improved PV-EM pipeline and our previous soft-segmentation work in removing the small bowel as well as the remaining bone. The pictures at the top row are segmentation results from our improved pipeline and the results obtained by our previous work are shown in the bottom row.

5. CONCLUSIONS

Partial-volume image segmentation for directly quantifying the tissue mixture in each image voxel has been a more challenging task over the previous hard and soft image segmentations. This paper provides an accurate PV image model based on the data Gaussian statistics with continuous mixture values $0 \le Z_{ik} \le 1$. The parameter estimation by the EM algorithm is both theoretically attractive and practically useful. It has the potential to mitigate the PV effect of positive contrast tagging in CTC application, and provides improved endoscopic view quality and quantitative CAD measure.

ACKNOWLEDGEMENT

This work was supported in part by the NIH National Cancer Institute under Grant # CA082402 and Grant # CA110186. Dr. Lu was supported by the National Nature Science Foundation of China under Grant 30470490.

REFERENCES

[1] J. Reed and D. Johnson, "Automatic segmentation, tissue characterization, and rapid diagnosis enhancements to the CT colonoscopy analysis workstation", *Journal of Digital Imaging*; **10**: 70-73, 1997.

[2] Z. Liang, D. Chen, B. Li, A. Kaufman, M. Wax, and A. Viswambharan, "On segmentation of colon lumen for virtual colonoscopy", *SPIE Medical Imaging*; **3660**: 270-278, 1999.

[3] P. Pickhardt, R. Choi, I. Hwang, J. Butler, M. Puckett, H. Hildebrandt, R. Wong, P. Nugent, P. Mysliwiec, and W. Schindler, "Computed tomographic virtual colonoscopy to screen for colorectal neoplasia in asymptomatic adults", *New England Journal of Medicine*; **349**: 2191-2200, 2003.

[4] Z. Liang, F. Yang, M. Wax, J. Li, J. You, A. Kaufman, L. Hong, H. Li, and A. Viswambharan, "Inclusion of *a priori* information in segmentation of colon lumen for 3D virtual colonoscopy", *Conference Record of IEEE Nuclear Science Society and Medical Imaging Conference*: in CD-ROM, 1997.

[5] D. Chen, Z. Liang, M. Wax, L. Li, B. Li, and A. Kaufman, "A novel approach to extract colon lumen from CT images for virtual colonoscopy", *IEEE Transactions on Medical Imaging*; **19**: 1220-1226, 2000.

[6] L. Li, D. Chen, S. Lakare, K. Kreeger, I. Bitter, A. Kaufman, M. Wax, P. Djuric, and Z. Liang, "An image segmentation approach to extract colon lumen through colonic material tagging and hidden Markov random field model for virtual colonoscopy", *SPIE Medical Imaging*, **4683**: 406-411, 2002.

[7] Z. Wang, Z. Liang, L. Li, X. Li, B. Li, J. Anderson, and D. Harrington, "Reduction of false positives by internal features for polyp detection in CT-based virtual colonoscopy", *Medical Physics*, **32**: 3602-3616, 2005.

[8] Z. Liang, Z. Wang, B. Li, and H. Lu, "Improved electronic colon cleansing with less-stressful bowel preparation for computer-aided detection of polyps in CT colonography", *The 91st Annual Meeting of the Radiological Society of North America (RSNA)*, pp.440, 2005.

[9] Z. Wang, Z. Liang, X. Li, L. Li, B. Li, D. Eremina, and H. Lu, "An improved electronic colon cleansing method for detection of colonic polyps by virtual colonoscopy", *IEEE Transactions on Biomedical Engineering*; **53**: 1635-1646, 2006.

[10] H. Choi, D. Haynor, and Y. Kim, "Partial volume tissue classification of multichannel magnetic resonance images – a mixel model", *IEEE Transactions on Medical Imaging*; **10**: 395-407, 1991.

[11] P. Santago and H. D. Gage, "Statistical models of partial volume effect", *IEEE Transactions on Image Processing*; **4**: 1531-1539, 1995.

[12] K. Leemput, F. Maes, D. Vandermeulen, and P. Suetens, "A unifying framework for partial volume segmentation of brain MR images", *IEEE Transactions on Medical Imaging*; **22**: 105-119, 2003.

[13] Z. Liang, X. Li, D. Eremina, and L. Li, "An EM framework for segmentation of tissue mixtures from medical images", *Proceeding of the International Conference of IEEE Engineering in Medicine and Biology*, pp. 682-685, Cancun, Mexico, 2003.

[14] D. Eremina, X. Li, W. Zhu, J. Wang, and Z. Liang, "Investigation on an EM framework for partial volume image segmentation", *SPIE Medical Imaging*, **6144**: D1-D9, 2006.

[15] A. Dempster, N. Laird, and D. Rubin, "Maximum likelihood from incomplete data via the EM algorithm", *J. R. Stat. Soc.*, **39**(B): 1-38, 1977.

[16] Z. Liang, R. Jaszczak, and E. Coleman, "Parameter estimation of finite mixtures using the EM algorithm and information criteria with application to medical image processing", *IEEE Transactions on Nuclear Science*, **39**: 1126-1133, 1992